

AD-A101 066

NATIONAL AERONAUTICS AND SPACE ADMINISTRATION CLEVEL--ETC F/G 21A  
COLD-AIR PERFORMANCE OF COMPRESSOR-DRIVE TURBINE OF DEPARTMENT --ETC(1)  
JUN 81 R J ROELKE, J E HAAS EC-77-A-31-1011

UNCLASSIFIED

NASA-TM-81932-1

USAFAVRADCOM-TR-R0-C-20-1 NL

Line 2  
SLOW

END  
7/21  
DTC

CONT.

ADA101066

NASA

AVRADCOM

Technical Memorandum 81932 Technical Report 80-C-20

**Cold-Air Performance of Compressor-  
Drive Turbine of Department of Energy  
Upgraded Automobile Gas Turbine Engine**

**I - Volute-Manifold and Stator Performance**

**Richard J. Roelke**  
*Lewis Research Center*  
*Cleveland, Ohio*

**Jeffrey E. Haas**  
*Propulsion Laboratory*  
*AVRADCOM Research and Technology Laboratories*  
*Lewis Research Center*  
*Cleveland, Ohio*



National Aeronautics  
and Space Administration

**Scientific and Technical  
Information Branch**

1981

**NOTICE**

This report was prepared to document work sponsored by the United States Government. Neither the United States nor its agent, the United States Department of Energy, nor any Federal employees, nor any of their contractors, subcontractors or their employees, makes any warranty, express or implied, or assumes any legal liability or responsibility for the accuracy, completeness, or usefulness of any information, apparatus, product or process disclosed, or represents that its use would not infringe privately owned rights.

Accession For	
NTIS GRA&I	<input checked="" type="checkbox"/>
DTIC TAB	<input type="checkbox"/>
Unannounced	<input type="checkbox"/>
Justification	
By _____	
Distribution/	
Availability Codes	
Dist	Avail and/or Special
<b>A</b>	

## Summary

The aerodynamic performance of the inlet manifold and stator assembly of the compressor-drive turbine of the Upgraded Gas-Turbine Engine was experimentally determined with cold air. The investigation included measurements of mass flow and stator-exit fluid torque over a range of pressure ratios. Radial surveys of stator-inlet total pressure and flow angle were taken at three stator pressure ratios, and annular surveys of stator-exit total pressure and flow angle were taken at two stator pressure ratios. The radial variations in aftermixed flow angle and efficiency were obtained, and the overall stator efficiency calculated. The overall efficiency thus obtained, was compared with the design value for this stator. In addition, the constituents of the total loss in stator kinetic energy were compared with the test results of three other reference stators.

The loss in total pressure in the inlet manifold ranged from 0.4 to 0.5 percent; however, the design swirl was not achieved near the endwalls. The undeturning of the flow near the endwalls resulted in positive stator incidence as high as 19° at one circumferential position. Measurements also indicated a thick hub boundary layer at the stator inlet.

The aftermixed stator efficiency between 20 and 90 percent span was generally equal to the design value of 0.965 but fell off appreciably at the endwalls. The overall aftermixed efficiency calculated for that part of the span surveyed (7 to 95 percent) was 0.959. An extrapolation of the survey measurements to the endwalls was made in an attempt to include the endwall losses. The overall aftermixed efficiency calculated from the extrapolated data was 0.936. An analysis of the factors contributing to the overall loss in kinetic energy (1 - efficiency) showed the following elements: profile, trailing-edge drag, and mixing, 0.035; incidence, 0.006; endwall boundary layer, 0.010; and secondary flow, 0.014. Comparison of the subject stator with another small stator and two larger stators showed that the small stators had comparable kinetic energy losses which were 50 to 100 percent more than the larger stators.

## Introduction

The Department of Energy (DOE) is sponsoring an engine research program to demonstrate an automobile powered by a gas-turbine engine of contemporary design with drivability characteristics and fuel economy that can compete with a conventionally powered automobile. A DOE (at that time the Energy Research and Development Administration) contract was awarded to the Chrysler Corporation to design, build, and road demonstrate this Upgraded Gas-Turbine (UGT) engine. A general description and some of the design features of the upgraded engine are given in reference 1. NASA, under an interagency agreement with DOE, was assigned the tasks of aerodynamically designing and testing the turbomachinery components.

The turbomachinery components designed and under evaluation at the Lewis Research Center include the compressor, compressor-drive turbine, and power turbine. The aerodynamic designs of these components are described in references 2, 3, and 4. The aerodynamic design of the compressor-drive turbine-inlet manifold and the mechanical designs of all the turbomachinery components were performed by the Chrysler Corporation.

This report presents the results of the experimental evaluation of the inlet manifold and stator assembly of the compressor-drive turbine. The investigation was made to determine (1) the losses within the manifold, (2) the flow conditions entering and leaving the stator, and (3) the stator blading performance. The aerodynamic evaluation of the manifold and stator will subsequently be used for evaluating the turbine rotor performance from overall stage data.

The performance of the manifold-stator assembly was determined with air at a nominal inlet temperature of 300 K and inlet pressures from 110 to 270 kPa. The investigation included circumferential measurements of mass flow and stator-exit fluid torque over a range of pressure ratios, radial surveys of stator-inlet total pressure and flow angle at three circumferential locations and three pressure ratios,

and annular surveys of stator-exit total pressure and flow angle at two stator sectors and two pressure ratios.

This report includes a description of the inlet manifold and stator, the experimental procedures used, and the experimental results. The radial variations in the manifold total pressure loss and manifold-exit (stator inlet) flow angle are presented. The variation in stator loss and exit flow conditions with circumferential and radial positions are also presented, and the overall stator efficiency calculated. Comparisons are made between the test results and design of the manifold-exit flow conditions, mass flow, stator-exit flow angle, exit fluid torque, and efficiency. A comparison is also made between the subject stator performance and three other stators tested at the Lewis Research Center.

## Symbols

$A$	area, $\text{m}^2$
$e$	kinetic energy loss coefficient, $(1 - \eta)$ or $(1 - \bar{\eta})$
$m$	mass flow rate, $\text{kg/sec}$
$P$	pressure, $\text{Pa}$
$R$	gas constant, $\text{J/kg K}$
$r$	radial location, $\text{m}$
$T$	temperature, $\text{K}$
$V$	velocity, $\text{m/sec}$
$\alpha$	flow angle measured from axial direction, deg
$\gamma$	ratio of specific heats
$\delta$	ratio of inlet total pressure to U.S. standard sea-level pressure, $P_{4,5}/P^*$
$\epsilon$	function of $\gamma$ used in relating parameters to those using air inlet conditions at U.S. standard sea-level conditions, $(0.740/\gamma)[(\gamma + 1)/2]^{1/\gamma - 1}$
$\eta$	aftermixed efficiency at radius $r$ based on kinetic energy
$\bar{\eta}$	overall aftermixed efficiency based on kinetic energy
$\theta_{cr}$	squared ratio of critical velocity at turbine inlet temperature to critical velocity at U.S. standard sea-level temperature, $(V_{cr}/V_{cr}^*)^2$
$\mu$	viscosity, $\text{N s/m}^2$
$\rho$	density, $\text{kg/m}^3$
$\tau$	torque, $\text{N m}$

$\psi$  mass flow parameter,  $(\frac{\Delta m_{local}}{\Delta m_{av}} - 1)$

Subscripts:

$av$	average
$cr$	flow conditions at Mach 1
$eq$	equivalent
$i$	survey position closest to inner (hub) wall
$id$	ideal or isentropic
$m$	mean
$o$	survey position closest to outer (tip) wall
$u$	tangential direction
$x$	axial direction
4.5	station at manifold inlet (fig. 5)
5.0	station at manifold exit (fig. 5)
5.5	station at stator exit (fig. 5)
5.5M	station downstream of vane trailing edge where flow is assumed to be circumferentially uniform (fig. 5)

Superscripts:

'	total state condition
*	U.S. standard sea-level conditions (temperature, 288.15 K; pressure, 101.3 kPa)

## Apparatus and Instrumentation

### Inlet-Manifold and Stator Description

A cross section of the upgraded compressor-drive turbine (UCT) is shown in figure 1. It is a single stage, axial-flow design with a stator tip diameter of 11.13 cm and a stator height of 1.12 cm. The design mass flow rate is 0.598 kg/s and the inlet temperature

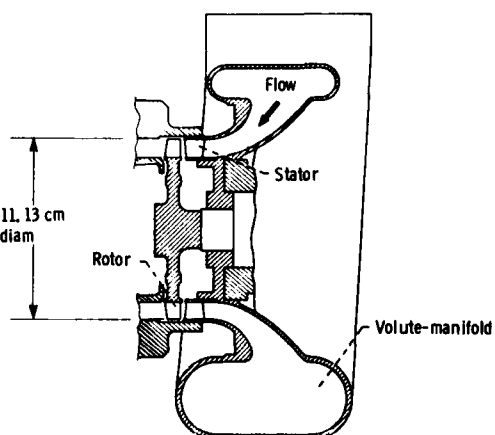


Figure 1 - Cross section of compressor-drive turbine.

and pressure are 1325 K and 397 bars absolute. The hardware used for the experiment described herein consisted of the inlet manifold and stator ring.

A photograph of the inlet manifold and stator installed in the test stand is shown in figure 2. Air enters the volute-shaped manifold by way of a single-entry port where swirl is imparted to the flow. The swirling flow leaves the volute and is accelerated in an axisymmetric duct to the stator inlet. The design intent for the inlet manifold was to establish free vortex flow conditions at the stator inlet. At the stator mean radius the design critical velocity ratio,  $(V/V_{cr})_5$ , is 0.403, and the flow angle,  $\alpha_5$ , is 48.7°.

The stator was designed to turn the flow an additional 17.6° at the mean to an exit angle of 66.3° and to accelerate the flow to a velocity ratio of 0.929. There are 15 stator vanes. The stator aspect ratio is 0.484, and the mean radius solidity is 1.103. The incompressible Zwiebel coefficients (ref. 5) are 0.568, 0.664, and 0.745 at the hub, mean, and tip, respectively. The stator design efficiency, based on an experimental correlation, was assumed radially constant at 0.965. Figure 3 shows the stator mean radius profile and velocity vectors. Additional stator details are contained in reference 3. Both manifold and stator used in the test were cast engine parts.

#### Research Facility Description

The experimental apparatus consisted of the research hardware, the air supply system, and the flow control valves. A diagram of the experimental installation and a cross-sectional view of the research rig are shown in figures 4 and 5. Dry pressurized room-temperature air from a central supply system

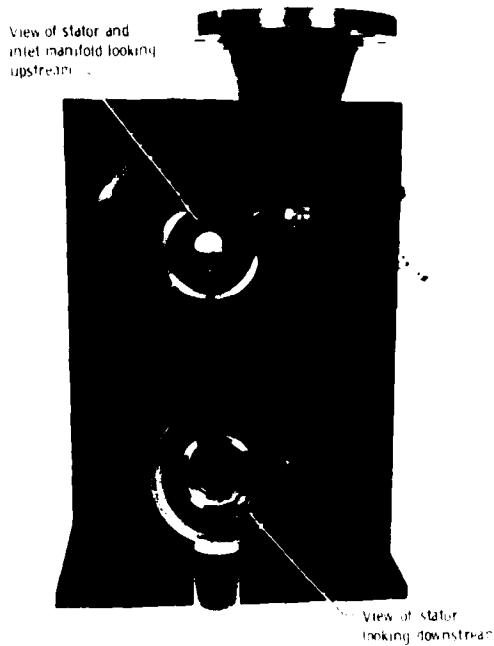


Figure 2. - Inlet-manifold and stator test hardware.

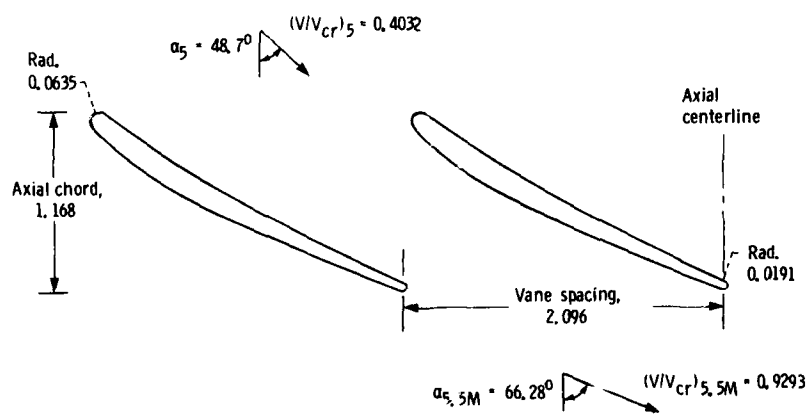


Figure 3. - Mean-radius stator profiles, flow passage and velocity vectors  
(Dimensions in centimeters).

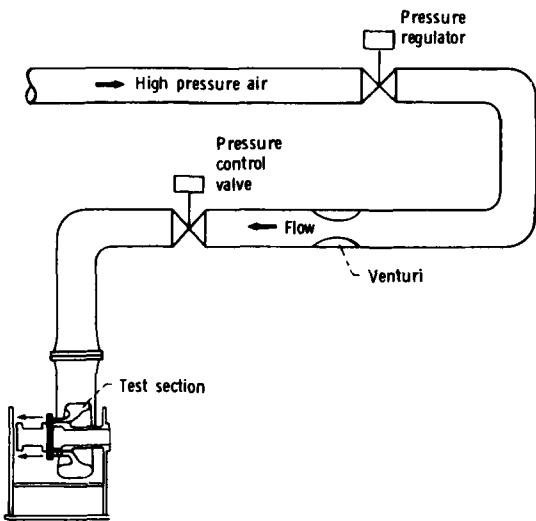


Figure 4. - Test installation diagram.

flowed through the test section and was exhausted into the room. A pressure control valve at the inlet was used to set the flow conditions. The air flow was measured with a calibrated venturi.

#### Instrumentation

Figure 6 shows the station nomenclature and the instrumentation used to measure wall static pressure, total temperature, total pressure, and flow angle. Figure 5 shows the axial locations of the stations. Instrumentation at the manifold inlet (station 4.5) measured total pressure, static pressure, and total temperature. The temperature and total pressure were measured with three rakes. Two of these rakes contained two pressure probes and one thermocouple. The third rake contained two thermocouples and one pressure probe.

At the stator inlet (station 5), located approximately 0.60 centimeter upstream of the stator, the static pressure, total pressure, and flow angle were measured. Static pressures were obtained from 10 taps with 5 on the inner wall and 5 on the outer wall of the annulus. Combination radial traversing probes, located midway between adjacent stator vanes, at locations A, B, and C were used to determine the radial variation in total pressure and flow angle. A photograph of this probe is shown in figure 7. The probe consisted of three parallel stainless-steel tubes. The center tube had an outside diameter of 0.050 centimeter and was used to measure total pressure. The side tubes had outside diameters of 0.038 centimeter and had the sensing

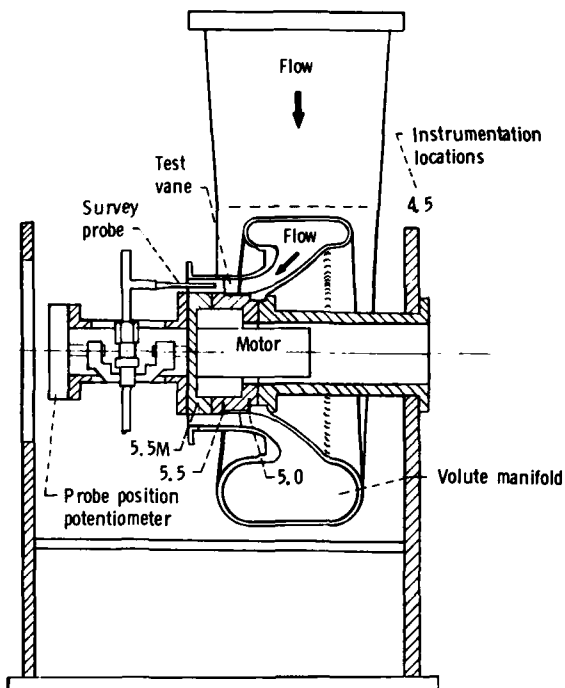


Figure 5. - Schematic cross-section of the volute-manifold stator test rig used for survey tests.

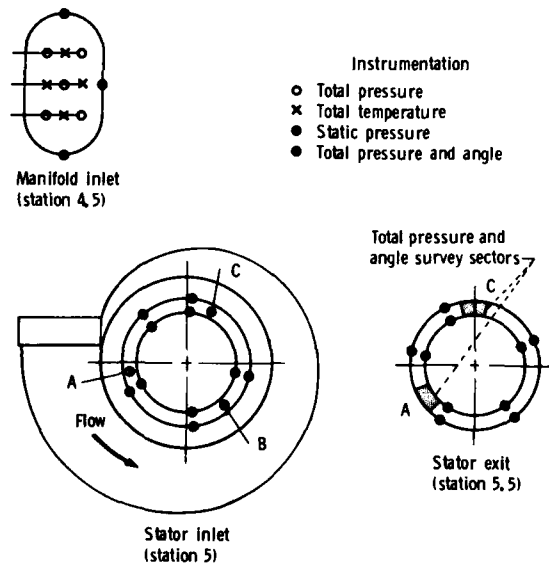


Figure 6. - Flow path measurements, viewed looking downstream.

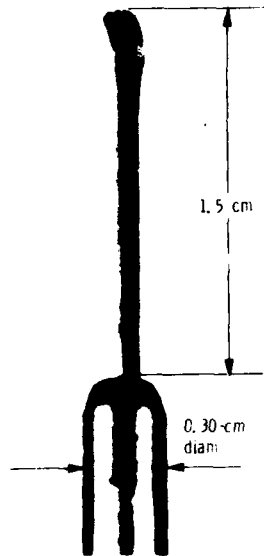


Figure 7. - Stator inlet survey probe.

ends cut off at  $45^\circ$  angles to measure the flow angle. These probes were positioned at a fixed angle, and the total pressure and flow angle were determined from calibration curves.

At the stator exit (station 5.5), located 0.25 centimeter downstream of the stator trailing edge, the static pressure, total pressure, and flow angle were measured. Static pressures were obtained from 10 taps with 5 on the inner wall and 5 on the outer wall of the annulus. Two survey probes of similar design were used to determine the radial and circumferential variations in total pressure and flow angle in annular sectors A and C. Sectors A and C correspond to the stator-inlet survey locations A and C, respectively. A photograph of one of the stator-exit survey probes is shown in figure 8. The difference between the two probes used was the downward angle of the sensing end of the three tubes. A single probe could not be used to survey along the entire stator height because of the high curvature of the hardware. A probe with the sensing tip bent  $20^\circ$  was used to survey from the hub to about 40 percent stator height and a probe bent  $11^\circ$  was used to survey from about 20 percent stator height up to the tip. Good agreement in both measured total pressure and flow angle was obtained from the two probes where they overlapped. As shown in the insert of figure 8, the probe had a single tube to measure the total pressure which was located underneath and slightly ahead of the two tubes used to measure the flow angle. The top two tubes had their sensing ends

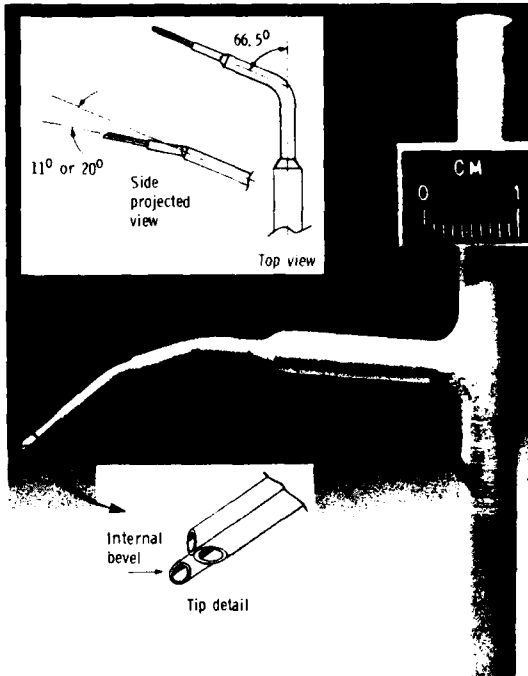


Figure 8. - Stator-exit survey probe.

cut off to form a  $90^\circ$  wedge. Each of the three stainless-steel tubes had an outside diameter of 0.038 centimeter. In both annular sectors the probe was positioned at a fixed angle and the total pressure and flow angle were determined from calibration curves.

All research pressures were measured with unbonded, strain-gage transducers. The electrical signals from the pressure transducers as well as the temperature readouts were measured and recorded by a 200-channel data-acquisition system.

## Procedure

The stator performance evaluation consisted of a measurement of the mass flow, surveys of total pressure and flow angle at the stator inlet and exit, and a measurement of the stator-exit fluid torque. The stator tests were conducted at nominal inlet conditions of 300 K and pressures that ranged from 110 to 270 kPa, absolute. The variation in inlet pressure was required to set the rig pressure ratio since the stator exit was open to the room.

Stator inlet surveys (station 5) were conducted at the three circumferential positions shown in figure 6.

These surveys were conducted at values of manifold-inlet-total to stator-exit-static-pressure ratios of nominally 1.6, 1.8, and 2.0. The design equivalent pressure ratio was 1.81. At each circumferential position and for each pressure ratio, total pressure and flow angle data were obtained at 14 radii ranging from approximately 2 to 98 percent of the stator height.

The stator-exit fluid torque was measured with a set of flow-straightening vanes behind the stator. A cross-sectional view of the stator with the straightening vanes installed is shown in figure 9. In this concept the straightening vanes turn the stator-exit flow to the axial direction. Thus, the stator-exit tangential momentum is removed. The free-floating straightening vane section was connected to a commercial load cell. A buffered labyrinth was used to prevent leakage of stator flow around the straightening vanes. At the stator design pressure ratio a radial survey of flow angle made behind the straightening vanes indicated a small amount of residual fluid torque (about 1.6 percent of the amount measured by the load cell), which was added to the measured torque. Stator exit torque data were obtained over a range of manifold-inlet-total to stator-exit-static pressure ratio from 1.3 to 2.1.

Stator-exit surveys (station 5.5) were made at the two sectors shown in figure 6 at values of manifold-inlet-total to stator-exit-static pressure ratio of approximately 1.6 and 1.8. At each sector and for each pressure ratio, total pressure and flow angle data were obtained at several radii ranging from about 7 to 95 percent of the stator height. The

smallness of the hardware and small raised ridges between adjacent stator vanes left from the casting process did not permit getting measurements any closer to the endwalls. At each fixed radius the probe was moved circumferentially to cover the stator pitch ( $24^\circ$ ) with data being obtained at discrete points every  $1.2^\circ$ . At each discrete point the probe movement was stopped, and the probe pressures were allowed to reach equilibrium before taking the data.

## Data Reduction

The stator efficiency was calculated from the stator-exit surveys of total pressure and flow angle. In the calculation the static pressure was assumed to vary linearly between the hub and tip wall values.

The calculation of the stator efficiency is based on the determination of a hypothetical state where it is assumed that the flow has mixed to a circumferentially uniform condition (station 5.5M). At each radius the conservation of mass, momentum, and energy are used to obtain this aftermixed state (i.e.,  $V_{5.5M,x}$ ,  $V_{5.5M}$ ,  $T_{5.5M}$ ,  $\alpha_{5.5M}$ , etc.) from the survey measurements. The calculation procedure is described more fully in reference 6. The aftermixed efficiency is used herein because it is theoretically independent of the axial location of the survey measurement plane. It should be noted that the aftermixed efficiency contains not only the stator profile loss but also the mixing loss. The aftermixed flow conditions may then be directly compared with the stator design velocity diagrams and efficiency.

The stator aftermixed efficiency based on kinetic energy can be defined as a function of radius  $\eta_{5.5M}$ , or as an overall quantity  $\bar{\eta}_{5.5M}$  as given by the following equations from reference 6.

$$\eta_{5.5M} = \frac{V_{5.5M}^2}{V_{5.5M,id}^2}$$

$$\bar{\eta}_{5.5M} = \frac{\int_{r_i}^{r_o} \rho_{5.5M} V_{5.5M,x} V_{5.5M}^2 r dr}{\int_{r_i}^{r_o} \rho_{5.5M} V_{5.5M,x} V_{5.5M,id}^2 r dr}$$

where

$$V_{5.5M,id} = \left\{ \left( \frac{2\gamma}{\gamma-1} \right) R T'_{4.5} \left[ 1 - \left( \frac{P_{5.5M}}{P'_5} \right)^{(\gamma-1)/\gamma} \right] \right\}^{1/2}$$

With the equation for  $\bar{\eta}_{5.5M}$ , the integrations were made only over the radii surveyed from about 7 to 95 percent of the stator height.

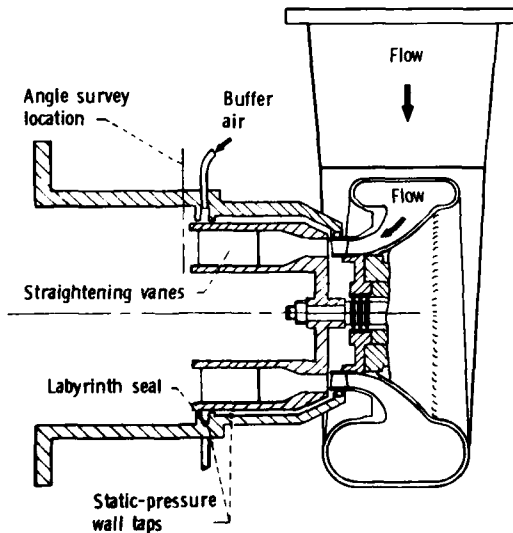


Figure 9. - Schematic cross-sectional view of test rig used to measure the stator-exit fluid torque.

To obtain an indication of the stator total loss, including the endwall regions, the flow measurements taken at the survey pressure ratio of 1.76 were extrapolated to the endwalls. Extrapolations of flow angle and total pressure that deviated only slightly from straight lines were made at both stator inlet and exit, with the total pressure at the endwalls set equal to the wall static pressure. Integrated values of mass flow and stator-exit fluid torque were calculated and compared with the same two parameters obtained by direct measurements to check the reasonableness of the extrapolations. Finally, the overall stator efficiency was calculated.

## Results and Discussion

This section presents the overall aerodynamic performance of the inlet manifold and stator. The measured mass flow of the manifold-stator assembly, the manifold flow characteristics, and the stator performance are presented. The stator performance is presented in terms of exit flow measurements, kinetic energy loss coefficients, and overall aftermixed efficiency. The results are compared with design values, and the stator kinetic energy loss coefficients are compared with three other stators.

### Mass Flow

The variation in equivalent mass flow with equivalent manifold-inlet-total to stator-exit-static pressure ratio is shown in figure 10. The design value of mass flow given in the figure is 2.8 percent less than the design equivalent mass flow listed in reference 3. This difference accounts for the

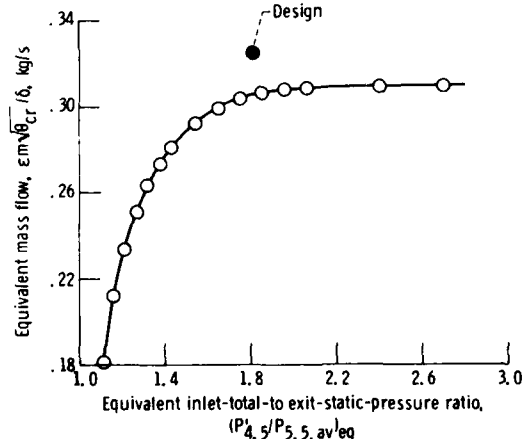


Figure 10. - Variation of equivalent mass flow with pressure ratio.

calculated thermal contraction in stator flow area between the engine temperature and rig temperature. At the design equivalent pressure ratio of 1.81 the measured mass flow was 0.306 kg/s which is 6 percent less than the design flow, 0.3256 kg/s, for a cold stator. Most of this deficit was caused by an undersized stator. The cold stator throat area was measured and found to be 4.1 percent small. The reduced flow area was caused by the size of the fillets and draft angles used in casting the stator and by a slightly shortened vane height. The remaining 1.9 percent deficit in mass flow was caused by higher than design aerodynamic losses.

### Manifold Flow Characteristics

Radial surveys of flow angle and total pressure were made at the manifold exit (station 5) at three circumferential locations (fig. 6) for pressure ratios of 1.56, 1.76, and 1.96. The survey results obtained at a manifold-inlet-total to stator-exit-static pressure ratio of 1.76 are shown in figure 11. The angle measurements are plotted in figure 11(a). The upper dashed line in the figure is the design radial variation in manifold-exit gas angle, and the lower dashed line is the radial variation in stator-inlet blade angle. As can be observed, the radial variation in the measured

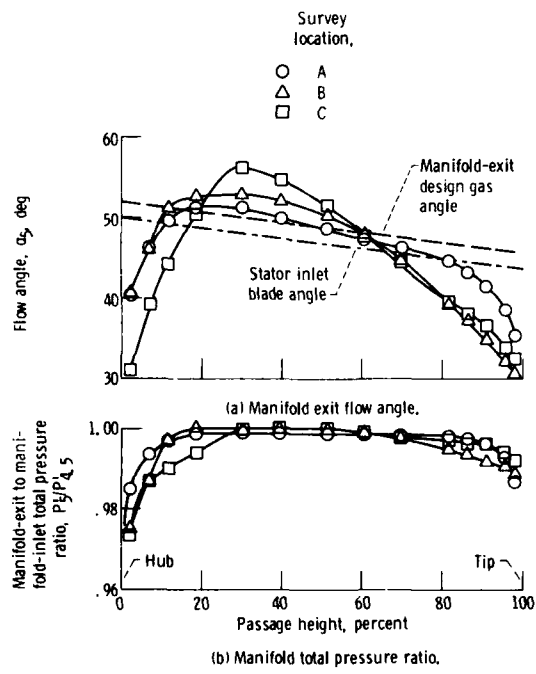


Figure 11. - Variation of manifold-exit flow angle and manifold total pressure ratio with radial position. Manifold-inlet-total to stator-exit-static pressure ratio, 1.76.

flow angle differed, depending on circumferential location, and near the endwalls differed substantially from the design intent. The flow angle variation at location *A* agreed best with design, while the flow angle variation at location *C* has the largest deviation from design. It is evident from figure 6 that the flow at *A* had the shortest spiraling flow path in the manifold and that the flow at *C*, the longest. It appears, therefore, that as the flow path in the volute manifold is increased the flow following that path becomes more distorted and varies the most from design.

Because of the distorted flow entering the stator, there is substantial positive incidence near the endwalls and greater than design negative incidence between 20 and 60 percent span. The stator incidence can be obtained by subtracting the measured flow angle from the stator angle. The largest incidence measured occurred at location *C*, where it varied from +19° at the hub to -8° at 30 percent span to +13.2° at the tip. The effect of this incidence on stator performance is discussed in a later section.

The radial variations in manifold-exit total pressure at the three survey locations are plotted in figure 11(b). The pressure variations indicate a very small total-pressure loss between 20 and 70 percent span. Near the endwalls, however, the loss in total pressure increases and indicates a thick boundary layer. The smallest pressure loss near the walls was measured at location *A*, whereas location *B* had the highest pressure loss near the tip wall, and location *C* had the highest pressure loss near the hub wall.

The radial variations in calculated mass flow at the three survey locations are shown in figure 12. The mass flows were calculated from the survey results and are expressed in terms of the mass flow parameter,  $\psi$ . The mass flow parameter is defined as

$$\psi = \frac{(\Delta m)_{\text{local}}}{(\Delta m)_{\text{av}}} - 1$$

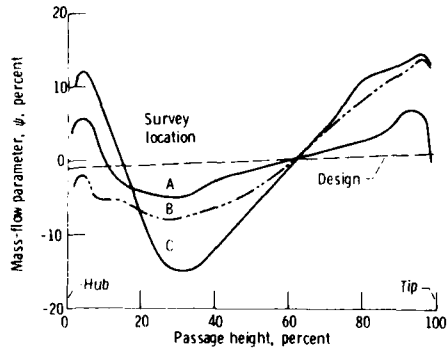


Figure 12. - Radial variation in mass flow parameter at the manifold exit (stator inlet).

and was used to provide nondimensionalized numbers because of the difference between the design and measured mass flows. The  $(\Delta m)_{\text{local}}$  was the calculated mass flow through each of 40 equal incremental flow areas. The  $(\Delta m)_{\text{av}}$  was the summation of the calculated local mass flows divided by 40. All of the calculations were made assuming a linear variation in static pressure from hub to tip. The mass flow parameter,  $\psi$ , indicates the percentage deviation in the local mass flow from the average mass flow at a given radial and circumferential location.

The total mass flow calculated for each of the three survey locations was nearly identical to each other but there was a wide variation in the radial distribution of mass flow. Figure 12 shows that for the design case the mass flow parameter varied from -1 percent at the hub to 1 percent at the tip. Compared with design, the calculated mass flow was lower between 15 and 60 percent of the annulus height for all three survey locations and was higher near both endwalls. The least difference between the minimum and maximum value of the mass flow parameter was at survey location *A*, and the largest difference was at survey location *C*. These trends were attributed to the flow turning more tangentially near midspan but not turning toward the tangential direction near the endwalls. The lower mass flow rate in the center of the manifold flow passage results in low flows through the high efficiency region of the stator. This result and the higher mass flow rate near the endwalls where the stator efficiency is lowest are believed to have a major detrimental effect on stator performance. Further, as will be shown in the stator performance section, higher stator losses were measured at location *C*, which had the most severe radial variation in inlet flow conditions.

The displacement and momentum thicknesses were calculated from the experimental data using the aforementioned extrapolations for the three survey locations and are tabulated in table I. As can be seen

TABLE I. - BOUNDARY-LAYER PARAMETERS  
AT THE MANIFOLD EXIT

[Calculated From Survey Measurements at station 5.]

	Survey location		
	A	B	C
Hub Displacement thickness, cm	0.013 .007	0.020 .012	0.029 .014
Tip Displacement thickness, cm	0.014 .006	0.019 .013	0.012 .005

from the values, the hub boundary layer thickened from location *A* to *C* as the flow moved through the volute. At the tip endwall, however, the boundary-layer parameters were generally the same at locations *A* and *C* but slightly higher at location *B*. The reason for this is not known. The total displacement thickness at location *A* was 2.5 percent of the radial height and 3.8 percent at location *C*.

A mass-averaged manifold total-pressure loss was also calculated from the extrapolated measurements. The calculated pressure losses were 0.4, 0.4, and 0.5 percent for locations *A*, *B*, and *C*, respectively.

As mentioned previously, manifold-exit surveys were made at three test pressure ratios. The survey data of flow angle and total pressure obtained at the other two pressure ratios (1.56 and 1.96) were nearly identical to the measurements at the 1.76 pressure ratio discussed above.

#### Stator Performance

**Stator-exit fluid torque.** — The stator-exit fluid torque was measured with straightening vanes for the range of pressure ratios from 1.35 to 2.10. These results are shown in figure 13. At the design equivalent pressure ratio of 1.81, the measured fluid torque was 3.93 newton-meters which is 7.9 percent less than design for the stator at room temperature. Part of this deficit (4.1 percent) is due to the low mass flow rate caused by the undersized stator throat area. The remaining 3.8 percent deficit is due to aerodynamic losses being higher than design. As discussed in an earlier section, the aerodynamic

losses caused a further reduction in mass flow of 1.9 percent. The remaining 1.9 percent deficit is due to a deficit in the moment of tangential momentum ( $rVu$ ). The reasons for the deficit in the moment of tangential momentum will be discussed with the survey results of the stator-exit flow conditions.

**Exit angle.** — The spanwise variations in stator aftermixed flow angle for the two sectors surveyed at a manifold-inlet-total to stator-exit-static pressure ratio of 1.76 are shown in figure 14. The measured radial variation in flow angle was similar for both sectors surveyed. The exit flow angle was less than design (the dashed line) near the endwalls and greater than design from 20 to 60 percent span. This pattern of undeturned flow near the endwalls and overturned flow in the midspan is similar to the stator-inlet flow-angle radial variation (fig. 11), that is, the radial variation in flow angle at the stator inlet persists through the stator. In the regions where the flow angle was less than design, the maximum difference measured was 3° at 7 percent span and 5° at 95 percent span; however, the flow angle likely has a greater difference in those areas nearer the endwalls that were not surveyed. The less than design-exit angle near the endwalls is one of the causes of the deficit in the moment of tangential momentum. In the region where the flow angle was greater than design the maximum difference was 3-1/2° at 35 percent span.

Although the exit flow angle was less than design near the endwalls, the endwall turning across the vane was greater than design. This is shown in figure 15 where turning across the vane is compared with the design turning. As can be seen, the radial locations where the flow was not turned at least equal to the design was from about 10 to 30 percent at location *A* and 20 to 60 percent at location *C*. The large area of undeturning indicated at location *C* is a result of the greater-than-design negative incidence at the stator inlet.

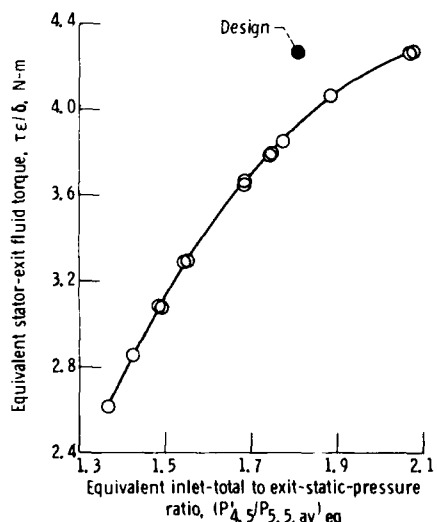


Figure 13. — Variation of equivalent-stator-exit fluid torque with pressure ratio.

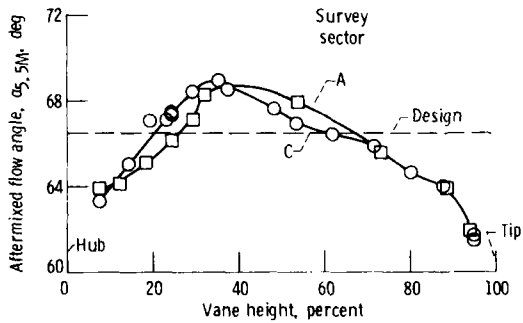


Figure 14. — Variation of stator-exit flow angle with radial position. Manifold-inlet-total to stator-exit-static pressure ratio, 1.76.

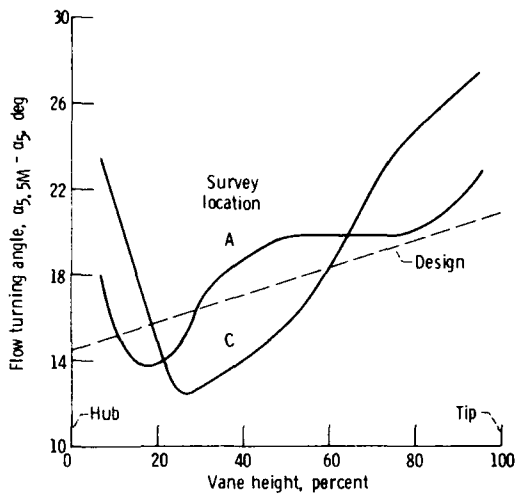


Figure 15. - Radial variation of change in flow angle across stator. Manifold-inlet-total to stator-exit-static pressure ratio, 1.76.

**Pressure ratio contours.** - A plot of the stator total-pressure-ratio contours, ( $P'_{S,5}/P'_S$ ), is shown in figure 16 for a single stator vane spacing at sector C at a manifold-inlet-total to stator-exit-static pressure ratio of 1.76. The projection of the stator trailing edge to the survey plane using experimental flow angles is also shown. From approximately 70 to 100 percent span, the distance between adjacent contours are greater on the suction surface side of the trailing-edge projection than on the pressure side. This suggests greater accumulation of low momentum flow in this region. Along the hub, a large loss area occurs from about midchannel between the vanes to the vane suction surface. It is likely that this is caused by the stator-inlet hub boundary layer flowing across the channel toward the suction surface.

**Efficiency.** - The radial variation in aftermixed efficiency at a pressure ratio of 1.76 for the two

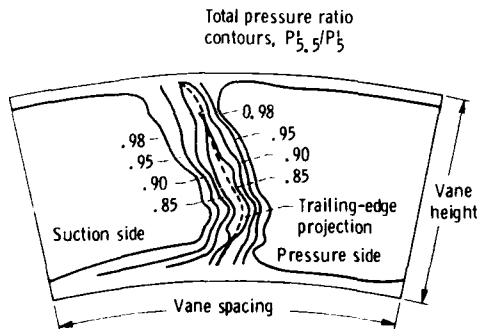


Figure 16. - Contours of stator total-pressure-ratio for sector C. Manifold-inlet-total to stator-exit-static pressure ratio, 1.76.

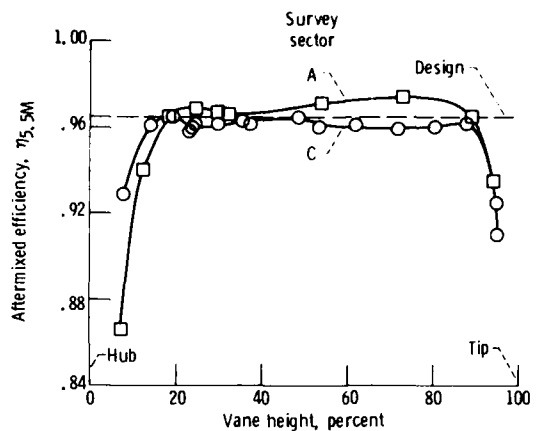


Figure 17. - Variation of stator efficiency with radial position. Manifold-inlet-total to stator-exit static pressure ratio, 1.76.

sectors surveyed is shown in figure 17. As explained in the Data Reduction section, the aftermix condition represents a hypothetical state where the flow has mixed to a circumferentially uniform condition. The efficiency thus obtained includes the flow mixing loss. The dashed line in the figure is the design efficiency.

Between 20 and 90 percent span the average experimental value of efficiency of the two sectors was 0.965. The efficiency in sector A was about 0.3 point higher than design, and the efficiency in sector C was about 0.3 point lower than design. The variation in stator incidence was highest in sector C and lowest in sector A, and therefore, was the probable cause of the decrease in efficiency. Near both endwalls the efficiency decreases rapidly in both sectors with the hub of sector A being lower than sector C. This decrease in efficiency near the endwalls reduces the magnitude of absolute velocity and is another cause of the deficit in the stator-exit moment of tangential momentum. It appears that between 20 and 90 percent span the difference in loss of the two sectors exists because of the difference in stator incidence; whereas near the endwalls the inlet boundary layer, augmented by the incidence effects at the stator inlet was the predominate loss mechanism. The overall aftermixed efficiencies were calculated between 7 and 95 percent span for both sectors and at two pressure ratios. The results are shown in table II. The difference in efficiency between the two sectors was 0.4 of a point.

**Results from extrapolation of survey measurements to the endwalls.** - The level of efficiencies determined in the preceding section would decrease with inclusion of the high losses at the endwalls. This was done by extrapolating the survey measurements to the endwalls realizing that

TABLE II. - STATOR AFTERMIXED EFFICIENCY

[Mass averaged values between 7 and 95 percent span.]

Manifold-inlet-total to stator-exit-static pressure ratio, $P_{4.5}/P_{5.5M}$	Stator aftermixed efficiency $\bar{\eta}_{5.5M}$	
	Sector A	Sector C
1.58	0.957	0.953
1.76	.961	.957

any extrapolation of the experimental data could introduce inaccuracies in the final results. The measurements taken at the survey pressure ratio of 1.76 for sectors *A* and *C* were individually extrapolated to the endwalls. Integrated values of mass flow, stator-exit fluid torque and overall mass averaged stator efficiency were calculated. The mass flow and stator-exit fluid torque calculated from the extrapolated survey results are compared to measurements to indicate the validity of the extrapolation.

The integrated mass flows for the two sectors were essentially the same and averaged 0.313 kilograms per second, which is 3 percent higher than the measured mass flow at the corresponding manifold-inlet-total to stator-exit-static pressure ratio. A change of only  $0.7^\circ$  in the stator exit flow angle would result in an integrated mass flow equal to the measured mass flow. This difference is within the accuracy of the stator-exit angle measurement.

The radial variation in mass flow parameter,  $\psi$ , calculated from stator-exit survey measurements and the design variation are shown in figure 18. As can be seen in the figure there was a substantial radial

variation in the calculated mass flow parameter at the stator exit which differed significantly from design. In general, the calculated stator-exit mass flow radial gradients were similar to those at the stator inlet. As was found at the stator inlet, the minimum mass flow (disregarding the regions immediately adjacent to the endwalls) occurred near midspan and the maximum mass flow occurred near the hub and tip. The lower mass flow near midspan and the higher mass flow near the endwalls contributes to lower overall stator efficiency.

The calculated stator-exit fluid torque obtained from the extrapolated stator-exit survey was very similar for the two sectors and averaged 3.86 newton meters. This value of torque was adjusted for the high integrated mass flow rate which, as previously discussed, was 3 percent above the measured value. At the corresponding pressure ratio, the fluid torque measured by the straightening vanes data was 3.84 newton meters, which is 0.5 percent less. The good agreement between the mass flow and stator-exit fluid torque obtained from the extrapolated survey data and the same two parameters obtained by direct measurements, indicates a reasonable extrapolation.

The overall mass-averaged stator efficiencies calculated were 0.937 and 0.935 for sectors *A* and *C*, respectively, compared with the design value of 0.965. As stated earlier, the stator efficiency for the annulus area, excluding the endwall regions, that is, the area from 20 to 90 percent span, averaged about 0.965. Therefore, the endwall regions contributed about 45 percent, that is,  $(0.965 - 0.936)/(1 - 0.936) = 0.45$ , of the total stator loss. Part of the stator endwall loss was caused by the flow conditions at the stator inlet (i.e., thick boundary layer and incidence effects), but the breakdown could not be determined from the tests conducted.

An estimate of the overall stator efficiency was also obtained by calculating a representative value of stator-exit velocity from stator-exit fluid torque and continuity. The tangential velocity component was calculated from stator-exit fluid torque using the mean radius and the measured mass flow rate. The axial velocity component was calculated from the mass flow measurement, the average measured static pressure at the stator exit, and the aerodynamic flow area. The aerodynamic flow area was calculated from the measured annulus area with adjustments made for stator trailing-edge blockage and vane profile and endwall displacement thicknesses. The overall stator efficiency calculated was 0.926, which agrees well with the value of 0.936 obtained from the stator survey. An estimate of the magnitude of the different loss contributors to the total stator loss is contained in the next section.

**Stator loss breakdown.** — The average total loss in kinetic energy  $(1 - \bar{\eta})$  for the stator sectors surveyed

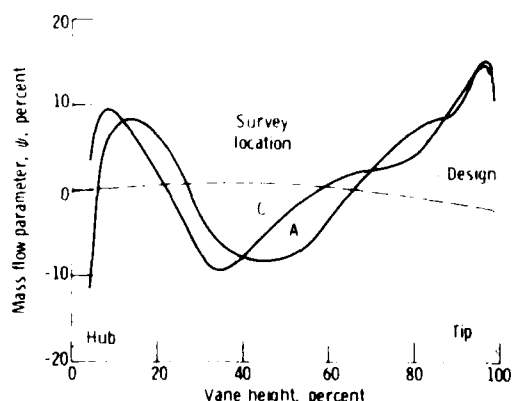


Figure 18. - Radial variation in mass flow parameter at the stator exit.

was determined to be 0.064 (1 - 0.936). From figure 17 it can be seen that the average kinetic energy loss at midspan was 0.035 (1 - 0.965), which is indicative of the profile, trailing-edge drag, and mixing losses. The difference between 0.064 and 0.035, that is, 0.029 is due to the losses that occur away from the mean radius. These losses include endwall friction, secondary-flow loss, and incidence. The contribution of each of these factors will now be discussed.

As stated earlier, the survey test results indicated a difference in the kinetic energy loss of about 0.006 between 20 and 90 percent span for sectors A and C and that differences in stator incidence was the most probable cause of this difference. The total incidence loss may be somewhat larger than 0.006 due to the higher incidence at the endwalls; however, it was not possible to experimentally separate the incidence loss from the other endwall losses. Empirical correlations of incidence loss were considered but they do not include boundary layer effects.

To obtain an estimate of the endwall friction loss, a procedure similar to that described in reference 7 was followed. The inviscid midchannel blade-to-blade free-stream velocities at the hub and tip endwalls were obtained using the TSONIC computer program (ref. 8). With these data the boundary-layer parameters on the endwalls were calculated with STANS (ref. 9), and the method of Stewart (ref. 10), as modified by Prust (ref. 11), was used to get the endwall friction loss. The endwall friction loss calculated was 0.01. The remaining stator loss of 0.013 (i.e., 0.029 - 0.006 - 0.01) is assumed to be

secondary flow loss. The loss breakdown is summarized below:

Loss at midspan (includes profile, trailing-edge drag, and mixing)	0.035
Incidence	0.006
Endwall friction	0.010
Secondary flow loss	0.013
Total aftermix loss	0.064

*Comparison with other stators.* — To better understand the sources of the increased losses in small stators, the current results were compared with test results of three other stators (ref. 7, 12, and 13). A brief physical description and loss breakdown of the four stators are listed in table III. All four stators were experimentally evaluated at Lewis with cold air under similar test procedures. The 76.2-and 50.8-centimeter-tip diameter stators were fabricated strictly for cold-air evaluation and were made by machining individual vanes and inserting them into hub and tip rings. This manufacturing method results in precisely controlled aerodynamic profiles with very smooth surface finishes and essentially no fillets at either endwall. Conversely, the GE-12 stator and the UCT stator were engine hardware parts. The GE-12 stator was fabricated by shaping and welding together several metal pieces into a two-vane segment. A full stator ring is then made by stacking segments together. The UCT stator was cast to final shape with no further machining to the flow path surfaces. As a result of the fabrication methods, the GE-12 and UCT stators did not have as smooth or

TABLE III. — COMPARISON OF STATOR TEST RESULTS

Stator	High temperature turbine (a)	Core turbine (b)	GE-12 (c)	UCT
Tip diameters, cm	76.2	50.8	19.0	11.1
Vane height, cm	10.16	3.81	1.75	1.09
Radius ratio	0.73	0.85	0.82	0.80
Aspect ratio	1.77	0.70	0.50	0.47
Trailing-edge blockage, percent	10	10	9.5	4.5
Critical velocity ratio ( $V/V_{cr}$ ) <sub>des,id</sub> at exit	0.79	0.78	0.89	0.96
Test Reynolds number, $m/\mu_m$	$5.1 \times 10^5$	$4.9 \times 10^5$	$3.4 \times 10^5$	$4.5 \times 10^5$
Kinematic energy loss coefficient, e:				
Mean radius	0.024	0.022	0.035	0.035
Endwall and secondary flow	0.010	0.018	0.036	0.024
Overall	0.034	0.040	0.071	d0.058

<sup>a</sup>Ref. 12.

<sup>b</sup>Ref. 7.

<sup>c</sup>Ref. 13

<sup>d</sup>Does not include incidence loss.

precisely controlled aerodynamic profiles as the two larger research stators.

Comparisons of the overall loss in kinetic energy ( $\epsilon$  overall) of the four stators showed that the two smaller stators had losses from 50 to 100 percent higher than the two larger research stators. Also, it can be noted that the increases in losses of the GE-12 and UCT stators resulted from increases in profile losses as well as increases in the endwall region losses. At the mean radius both small stators had the same kinetic energy loss, which was 0.011 to 0.013 higher than the larger stators. This larger loss cannot be attributed to high vane blockage because in this case the larger stators had higher blockage. The higher mean radius losses of the small stators may have been caused by one or both of the following conditions: (1) the skin friction loss of the GE-12 and UCT stators was significantly higher than the precisely made smooth surface finish research stators and (2) losses that were generated in the endwall regions of the small stators coalesced near midspan to increase the losses over the entire span. The latter condition was measured and reported in reference 14.

The increase in endwall losses of the small stators is expected and is most likely due to the higher ratio of endwall boundary layer to vane height. The largest endwall loss was measured for the GE-12 stator but this may have been caused by small discontinuities that occurred in the endwalls where adjacent stator segments abutted each other.

## Summary of Results

The aerodynamic performance of the inlet manifold and stator assembly of the compressor-drive turbine of the Upgraded Gas-Turbine Engine was experimentally determined in cold air. The investigation included measurements of mass flow and stator-exit fluid torque over a range of pressure ratios. Radial surveys of stator inlet total pressure and flow angle were taken at three stator pressure ratios, and annular surveys of stator-exit total pressure and flow angle were taken at two stator pressure ratios. The variation in stator efficiency and aftermixed flow conditions with radial position for two sectors of different circumferential location were obtained and compared with design values and three other tested stators. The results of the experiment are summarized as follows:

1. The measured mass flow was 6 percent less than design for a cold stator. Of this amount, 4.1 percent was due to an undersize throat and 1.9 percent was due to higher than design aerodynamic losses.
2. The measured total-pressure loss in the inlet manifold was only 0.4 to 0.5 percent; however, the

flow entering the stator was significantly undeturned near the endwalls, resulting in positive incidence as high as 19° at one circumferential location. In addition a thick hub boundary layer was measured entering the stator.

3. Large radial gradients in flow angle at the stator inlet resulted in higher than average mass flow near the walls and lower than average flow near midstream. This manifold mass-flow gradient became more severe as the distance from the manifold inlet increased.

4. The measured fluid torque at the stator exit was 7.9 percent less than design. Of this amount, 4.1 percent was due to low mass flow caused by an undersize stator throat area, and 3.8 percent was due to higher-than-design aerodynamic losses.

5. The average aftermixed stator efficiency of the two sectors between 20 and 90 percent span equalled the design value of 0.965, but fell off appreciably at the endwalls. The average overall aftermixed efficiency calculated for that part of the span surveyed (7 to 95 percent) was 0.959. When the measurements were extrapolated to the endwalls, the average value calculated was 0.936.

6. At design pressure ratio the stator vane loss (which includes profile, trailing-edge drag, and mixing losses) was experimentally determined to be 0.035, and the incidence and endwall region losses combined were 0.029. It was estimated that the stator incidence loss was 0.006 and the remaining 0.023 loss was due to endwall boundary layer and secondary flow losses. It was analytically determined that the endwall boundary layer loss was 0.010; therefore, the loss due to secondary flow was 0.013.

7. Comparison of the UCT stator with three other stators (one slightly larger and two significantly larger) showed that the two smaller stators had higher vane profile losses and much higher endwall losses. The larger vane profile losses of the two smaller stators were most likely caused by higher stator surface roughness than the larger stators and the migration of losses generated near the endwalls to the midspan thus increasing the losses over the entire vane height. The higher endwall losses were caused by boundary layers that were thick relative to the stator height and higher secondary flows.

## Concluding Remarks

The results obtained in this experimental investigation showed that the manifold and stator did not achieve their performance goals and that viscous flow effects may have been the main contributing factor. Apparently, the spiraling path the flow follows in the manifold generated thick boundary layers, which in turn significantly distorted both the

flow angle and radial mass flow distribution at the stator inlet. Therefore, a reduction in the manifold boundary layer should improve the radial gradients in flow angle and mass flow. It is believed that the stator-inlet boundary layer would be reduced by replacing the annular duct ahead of the stator with a bellmouth inlet. An optimum manifold, from an aerodynamic viewpoint, would probably require multiple inlets or a full annular inlet, although this may not be possible because of engine packaging constraints.

As was previously pointed out about half of the stator loss was contributed by the endwall regions. Design approaches, such as endwall contouring and increased solidity at the endwalls may minimize the high endwall losses and turn the flow more toward the tangential direction near the endwalls at the stator exit. These stator design changes and the design changes suggested for the manifold should redistribute the mass flow away from the endwalls and into the higher efficiency midspan region of the stator thus increasing the stator efficiency. While improvements in the design of the manifold and stator should reduce the endwall losses, these loss regions may still extend a significant distance from the endwalls. Therefore, a radial variation in efficiency should be used when designing small stators.

Lewis Research Center  
National Aeronautics and Space Administration  
Cleveland, Ohio, November 24, 1980

## References

1. Ball, G. A.; Oumaer, J. L.; and Sebestyen, T.M.: The ERDA Chrysler Upgraded Gas Turbine Engine Objectives and Design. SAE Paper 760279, 1976.
2. Roelke, Richard J.; and McLallin, Kerry L.: The Aerodynamic Design of a Compressor Drive Turbine for Use in a 75 kW Automotive Engine. NASA TM-71717, 1975.
3. Galvas, Michael R.: A Compressor Designed for the Energy Research and Development Agency Automotive Gas Turbine Program. NASA TM X-71719, 1975.
4. Kofskey, Milton G.; Katsanis, Theodore; and Schumann, Lawrence F.: Aerodynamic Design of a Free Power Turbine for a 75 kW Gas Turbine Automotive Engine. NASA TM X-71714, 1975.
5. Zweifel, O.: The Spacing of Turbo-Machine Blading, Especially With Large Angular Deflection. Brown Boveri Rev, vol. 32, no. 12, Dec. 1945, pp. 436-444.
6. Goldman, Louis J.; and McLallin, Kerry L.: Cold-Air Annular-Cascade Investigation of Aerodynamic Performance of Cooled Turbine Vanes, I - Facility Description and Base (Solid) Vane Performance. NASA TM X-3006, 1974.
7. Goldman, Louis J.; and McLallin, Kerry L.: Cold-Air Annular-Cascade Investigation of Aerodynamic Performance of Core-Engine-Cooled Turbine Vanes, I - Solid Vane Performance and Facility Description. NASA TM X-3224, 1975.
8. Katsanis, Theodore: FORTRAN Program for Calculating Transonic Velocities on a Blade-to-Blade Stream Surface of a Turbomachine. NASA TN D-5427, 1969.
9. Crawford, M. E.; and Kays, W. M.: STANS - A Program for Numerical Computation of Two-Dimensional Internal and External Boundary Layer Flows. NASA CR-2742, 1976.
10. Stewart, W. L.: Analysis of Two-Dimensional Compressible-Flow Loss Characteristics Downstream of Turbomachine Blade Rows in Terms of Basic Boundary-Layer Characteristics. NACA TN 3515, 1955.
11. Prust, H. W., Jr.: Boundary Layer Losses. Turbine Design and Application. Vol. II. NASA SP-290, 1973, pp 93-124.
12. Prust, Herman W., Jr.; Moffitt, Thomas P.; and Bider, Bernard: Effect of Variable Stator Area on Performance of a Single-Stage Turbine Suitable for Air Cooling. V-Stator Detailed Losses With 70-Percent Design Area. NASA TM X-1696, 1968.
13. Haas, Jeffrey E.; and Kofskey, Milton G.: Effect of Coolant Flow Ejection on Aerodynamic Performance of Low-Aspect Ratio Vanes, I - Performance With Coolant Ejection Holes Plugged. NASA TM X-3395, 1976.
14. Prumper, H.: Application of Boundary Fences in Turbomachinery. Boundary Layer Effects in Turbomachines, AGARD-AG-164, 1972, pp. 315-331.

1 Report No. NASA TM-81932 AVRADCOM TR 80-C-20		Government Accession No. <i>790-A101066</i>	
4 Title and Subtitle COLD-AIR PERFORMANCE OF COMPRESSOR-DRIVE TURBINE OF DEPARTMENT OF ENERGY UPGRADED AUTOMOBILE GAS TURBINE ENGINE I - VOLUTE-MANIFOLD AND STATOR PERFORMANCE		3. Recipient's Catalog No. <i>11</i>	
7 Author(s) Richard J. Roelke and Jeffrey E. Haas		5 Report Date June 1981	
9 Performing Organization Name and Address NASA Lewis Research Center and Propulsion Laboratory AVRADCOM Research and Technology Laboratories Cleveland, Ohio 44135		6. Performing Organization Code 505-32-2B	
12 Sponsoring Agency Name and Address U. S. Department of Energy Office of Transportation Programs Washington, D. C. 20545		8. Performing Organization Report No. E-572	
15 Supplementary Notes Richard J. Roelke, Lewis Research Center; Jeffrey E. Haas, AVRADCOM Research and Technology Laboratories. Prepared under DOE/NASA Interagency Agreement EC-77-A-31-1011		10. Work Unit No. <i>11</i>	
16 Abstract The aerodynamic performance of the inlet manifold and stator assembly of the compressor-drive turbine was experimentally determined with cold air as the working fluid. The investigation included measurements of mass flow and stator-exit fluid torque as well as radial surveys of total pressure and flow angle at the stator inlet and annulus surveys of total pressure and flow angle at the stator exit. The stator-exit aftermixed flow conditions and overall stator efficiency were obtained and compared with their design values and the experimental results from three other stators. In addition, an analysis was made to determine the constituent aerodynamic losses that made up the stator kinetic energy loss.		11. Contract or Grant No. <i>111-1111-1111-1111</i>	
17 Key Words (Suggested by Author(s)) Automotive gas turbine engine: Axial flow turbine: Stator aerodynamic performance: Viscous effects		13. Type of Report and Period Covered Technical Memorandum	
18 Distribution Statement Unclassified - unlimited STAR Category 02 DOE Category UC-96		14. Sponsoring Agency Code Report No. DOE/NASA/1011-34	
19 Security Classif. (of this report) Unclassified	20. Security Classif. (of this page) Unclassified	21. No. of Pages 13	22. Price* A02

*111-1111-1111-1111*  
For sale by the National Technical Information Service Springfield, Virginia 22161

~~CONFIDENTIAL~~

REF ID: A6572

DTIC

AD-A101 066

NATIONAL AERONAUTICS AND SPACE ADMINISTRATION CLEVEL--ETC F/G 21/5  
COLD-AIR PERFORMANCE OF COMPRESSOR-DRIVE TURBINE OF DEPARTMENT —ETC(U)  
JUN 81 R J ROELKE, J E HAAS EC-77-A-31-1011  
UNCLASSIFIED NASA-TM-82682-1 USAAVRADCOM-TR-80-C-20-1 NL

2 OF 2  
20  
4501060  
■

END  
DATE  
FILED  
10-81  
DTIC

**SUPPLEMENTARY**

**INFORMATION**

PO-A101 066

ERRATA

NASA Technical Memorandum 81932  
AVRADCOM Technical Report 80-C-20

COLD-AIR PERFORMANCE OF COMPRESSOR-DRIVE TURBINE OF DEPARTMENT  
OF ENERGY UPGRADED AUTOMOBILE GAS TURBINE ENGINE

I - VOLUTE-MANIFOLD AND STATOR PERFORMANCE

Richard J. Roelke and Jeffrey E. Haas  
June 1981

Cover, title page, and Report Documentation page, block 1 (last page):  
The NASA report number should be TM-82682.